

Logarithmically complex rigorous Fourier space solution to the 1D grating diffraction problem

¹Evgeniy Levdik and ²Alexey A. Shcherbakov

¹Univ. degli Studi di Siena, Siena, Italy

²ITMO University, St. Petersburg, Russia

2024

Abstract

The rigorous solution of the grating diffraction problem is a fundamental step in many scientific fields and industrial applications ranging from the study of the fundamental properties of metasurfaces to the simulation of lithography masks. Fourier space methods, such as the Fourier Modal Method, are established tools for the analysis of the electromagnetic properties of periodic structures, but are too computationally demanding to be directly applied to large and multiscale optical structures. This work focuses on pushing the limits of rigorous computations of periodic electromagnetic structures by adapting a powerful tensor compression technique called the tensor train decomposition. We have found that the millions and billions of numbers produced by standard discretization schemes are inherently excessive for storing the information about diffraction problems required for computations with a given accuracy, and we show that a logarithmically growing amount of information is sufficient for reliable rigorous solution of the Maxwell's equations on an example of large period multiscale 1D grating structures.

1 Introduction

The problem of simulating the diffraction of electromagnetic waves by wavelength-scale gratings can be solved efficiently by many methods [3]. However, when periodic structures have a multi-scale pattern, conventional rigorous numerical methods rapidly lose their efficiency as the largest scale and the difference between scales increase. As an example, consider a simple 2D structure with two characteristic scales Λ and Λ_1 , as shown in Fig. 1, where one has to finely resolve the fields in the region of size Λ_1 , which makes the total number of mesh nodes of length Λ quite large, provided that $\Lambda \gg \Lambda_1$. This is the case for metasurfaces, which typically represent 1D/2D periodic structures with complex unit cells and unique scattering properties [20]. As they move towards industrial applications, there is a growing need for the most appropriate and powerful simulation techniques.

There are several ways to address the problem of excessive complexity of rigorous electromagnetic computations.

The first is to develop hybrid and domain decomposition methods [4, 10, 11, 18, 8]. The second makes intensive use of modern machine learning (ML) methods [2, 13, 1, 25], with physics-informed neural networks in particular being among the most promising [14, 19]. Finally, there is a space in the implementation of the known methods taking into account the modern mathematical approaches, and the current work fits in this direction.

Fourier space methods such as the Fourier Modal Method (FMM), the Differential Method (DM), the C-Method or the Generalized Source Method (GSM) are among the most powerful for planar grating diffraction problems [17, 24, 5]. Among them, the GSM provides solutions with the lowest asymptotic complexity with respect to the Fourier space grid size N_F , namely $O(N_F \log(N_F))$. In essence, the GSM can be regarded as a Fourier space volume integral method. The fields are expressed as a superposition of plane waves. The volume integral equation, which provides a solution to the vector Helmholtz equation, can be reduced to a linear system of equations with an internal structure in the form of a product of block diagonal and block Toeplitz matrices [24, 23]. Although this method has demonstrated its efficiency for complex unit cells [22], it still requires too many computational resources for scales $\lambda \gg \lambda$, where λ is the wavelength.

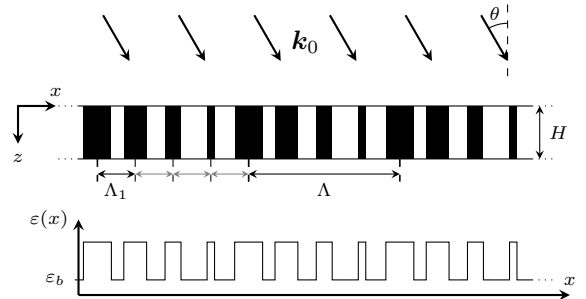


Figure 1: Plane wave diffraction on 1D grating with multi-scale pattern. Λ – grating period, Λ_1 – local characteristic scale. $\varepsilon(x, y, z) = \varepsilon(x, z)$ – grating dielectric permittivity spacial distribution periodic in x direction, \mathbf{k}_0 – incident wave vector, H – grating depth, θ – angle of incidence.

Since the GSM diffraction matrix has a regular structure, the corresponding calculations can be speeded up

dramatically for large matrix sizes. For this purpose, we propose to use the Tensor Train (TT) decomposition [15]. This is a low-rank tensor representation that allows storing vectors and matrices of size N with $O(\log N)$ elements. As well as being a way of compressing data, the TT format supports most tensor algebra operations, such as matrix and matrix-by-vector products. Linear systems of equations can be solved in TT format using the AMEn algorithm [15, 7]. So it's possible to solve an astronomically large linear system without ever calculating all its coefficients.

In this work we aim to investigate how an application of Tensor Train Decomposition within the GSM can speed up practical diffraction calculations. As a proof of concept, we focus on modelling diffraction by 1D gratings with multi-scale patterns. First, we describe an analytical model and review the equations to be solved numerically. Secondly, we introduce the tensor train format, relevant algorithms and describe how it has been applied within the GSM. Finally, we present the results of numerical simulations and evaluate the capabilities of the new method.

$$E_y(x, z) = E_y^{inc}(x, z) - \frac{\omega\mu_0}{4\pi^2} \int_{-\infty}^{\infty} d\zeta \int_{-\infty}^{\infty} dk_x e^{ik_x x} \frac{e^{ik_z|z-\zeta|}}{2k_z} \int_{-\infty}^{\infty} dx' J_y(x', \zeta) e^{-ik_x x'}. \quad (1)$$

Here the wavevector projections $k_{x,z}$ are related via the dispersion equation $k_z = \sqrt{k_0^2 - k_x^2}$, $k_0^2 = \omega^2 \varepsilon_0 \mu_0$.

To obtain a self-consistent equation the electric current is replaced by a generalized source $J_y^{gen} = -i\omega(\varepsilon(x) - \varepsilon_0)E_y$, which exists within the grating layer only, $-H/2 \leq z \leq H/2$. Then the Floquet-Bloch theorem is invoked and the Fourier decomposition of all periodic functions is applied. The field amplitude is replaced by a superposition of plane wave amplitudes propagating up and down with respect to their axis Z . Then, Eq. (1) for a fixed Bloch wavevector k_{x0} becomes

$$a_m^+(z) = a_m^{inc,+}(z) + \frac{ik_0^2}{2k_{zn}} \int_{-H/2}^z e^{ik_z(z-\zeta)} J_{my}^{gen}(\zeta) d\zeta \quad (2)$$

$$a_m^-(z) = a_m^{inc,-}(z) + \frac{ik_0^2}{2k_{zn}} \int_z^{H/2} e^{ik_z(\zeta-z)} J_{my}^{gen}(\zeta) d\zeta \quad (3)$$

with $k_{xm} = k_{x0} + 2\pi m/\Lambda$, $m \in \mathbb{Z}$.

Upon the Fourier transform the product $\Delta\varepsilon E_y$ becomes a convolution product. Discretizing the integral using the mid-point rule with the step h and the total number of z -slices N_S gives the infinite system of linear equations

$$a_{mk}^\pm = a_{mk}^{inc,\pm} + \frac{ik_0}{2k_{zn}} \sum_{q=1}^{N_S} \Theta_{m,kq}^\pm \sum_n \left(\frac{\Delta\varepsilon}{\varepsilon_0} \right)_{m-n} (a_{nq}^+ + a_{nq}^-) \quad (4)$$

2 The Generalized Source Method

The detailed derivation of the GSM in a general form can be found in [23, 24, 26]. Here we consider a simple 1D grating in vacuum. The diffraction problem is shown schematically in Fig. 1. The collinear monochromatic diffraction of TE polarised plane waves is considered for gratings of depth H with period Λ , and the period is assumed to be "pixelated" with pixel size Λ_1 and filling factor varying between pixels. The Cartesian coordinates are chosen so that the periodicity direction is along the axis X and the axis Z is perpendicular to the grating plane. The periodic permittivity depends only on the x coordinate, $\varepsilon = \varepsilon(x)$, so the grating is a 1D photonic crystal slab.

The solution of the vector Helmholtz equation for the electric field is written as a volume integral equation with the free space Green's dyadic [6]. In the simplest case of TE polarization at the plane wave decomposition, this solution takes the following form:

where

$$\Theta_{m,kq}^\pm = \frac{k_0 h}{2} \left[(1 - \delta_{kq}) e^{\pm ik_{zm} h (k-q)} + \delta_{kq} e^{ik_{zm} h / 2} \right] \theta(\pm(k-q)) \quad (5)$$

is written via the Kronecker δ -symbol and the Heaviside step function θ . Truncation of the infinite Fourier series, $|n| < N_F/2$, gives the system of linear algebraic equations, which we write through a specific matrix products:

$$\mathbf{a} = \mathbf{a}^{inc} - P_b Y D X \mathbf{a} \quad (6)$$

The size of the system is $2N_F N_S$. The block-diagonal matrices X and Y denote the forward and backward translation from the plane wave amplitudes to the Fourier amplitudes of the electric field projection y ; the block Toeplitz matrix D can be interpreted as an emission in each slice from the generalized sources; and the block diagonal matrix P_b describes the propagation of the emitted plane waves between the slices within the grating layer.

3 Tensor Train Decomposition

Tensor Train Decomposition is a method of storing tensors, including vectors and matrices, in a compact way. The TT format supports all basic operations of tensor arithmetic (summation, transposition, element-wise product, etc.), i.e. the result of an operation in TT format can be found by manipulating TT-formatted arguments without decompressing them [15]. This format, along with

many related algorithms, is implemented in the `tppy` library for Python by Ivan Oseledets, which we used for our calculations. For the sake of consistency, we outline below the basic definitions and algorithms that are essential for our simulations.

3.1 Definition and basic properties

A d -dimensional tensor T of size $n_1 \times \dots \times n_d$ is said to be in TT format if there exist d 3D tensors \mathcal{T}_k of size $r_{k-1} \times n_k \times r_k$, where $k = 1 \dots d$, such that:

$$T_{i_1 i_2 \dots i_d} = \mathcal{T}_1(i_1) \cdot \mathcal{T}_2(i_2) \cdot \dots \cdot \mathcal{T}_d(i_d) \quad (7)$$

3D tensors \mathcal{T}_k are called *cores*, and their sizes r_k are called *ranks* where $r_0 = r_d = 1$. $\mathcal{T}_k(i_k)$ are 2D slices of cores and « \cdot » stands for matrix multiplication. Since $r_0 = r_d = 1$, the first slice is a row vector and the last slice is a column vector, thus the resulting product is a scalar. This definition is visualized in Fig. 2.

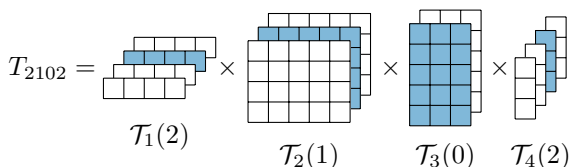


Figure 2: Illustration of the TT decomposition. Highlighted matrices are being multiplied to get an element of a 4D tensor of size $4 \times 3 \times 2 \times 4$. Indexing starts from zero.

If $r = \max(r_k)$ and $n = \max(n_k)$, the TT representation of a tensor has $O(dr^2n)$ elements, while the initial tensor has $N = O(n^d)$ elements. The ranks r_k do not depend on the size of the tensor. For any tensor, the ranks can be large and the TT format can be larger than the initial tensor. However, if a tensor is regularly structured, a representation with very small ranks can often be found. Furthermore, if an exact decomposition is not required and a low-rank approximation is allowed, the TT format can be very compact. If r is constant for any d , then the size of the TT decomposed tensor is proportional to $d \sim \log(N)$.

3.2 Matrices and vectors in TT format

The larger the dimension of the tensor, the more efficient its compression in TT format. However, most common tensors in numerical analysis are 2D (matrices) and 1D (vectors). To achieve logarithmic compression, matrices and vectors are reshaped into multidimensional tensors before decomposition [15].

A vector \mathbf{x} of size $N = n_1 \cdot \dots \cdot n_d$ is said to be in TT format if it is treated as a d -dimensional tensor $X_{i_1 \dots i_d}$ with mode sizes n_k , and this tensor is in the TT format. For simplicity, multi-index notation is used, i.e. the indices of a tensor can be treated as a *long* index and vice versa. i_1 is the slowest changing outer index, and i_d is the fastest changing inner index. The relation between i and i_k is as

follows:

$$i = i_1 N_{d-1} + i_2 N_{d-2} + \dots + i_{d-1} N_1 + i_d \quad (8)$$

where $N_k = n_1 \cdot \dots \cdot n_k$. For simplicity, the indexing starts at zero. The reverse calculation can be done iteratively with integer division and modulus.

Matrices in TT format are a bit more complicated, which is motivated by the need for a matrix-by-vector product algorithm that can work with TT formats without expanding tensors to full size. A matrix \mathbf{A} of size $N \times M$ is said to be in TT format if $N = n_1 \cdot \dots \cdot n_d$, $M = m_1 \cdot \dots \cdot m_d$, and:

$$\mathbf{A}_{ij} = A_{i_1 \dots i_d, j_1 \dots j_d} = \mathcal{A}_1(i_1 j_1) \cdot \dots \cdot \mathcal{A}_d(i_d j_d), \quad (9)$$

where either $i_k j_k$ is treated as a long index or the cores \mathcal{A}_k are treated as 4D tensors. This definition implies that N and M can be factorized with the same number of factors d . If this is not the case (for non-square matrices), it is still possible to define TT format by simply setting the excessive n_k or m_k to 1.

For such matrices and vectors reshaped into multidimensional tensors of the corresponding shapes, there are algorithms that perform matrix-by-vector and matrix-by-matrix multiplication [15], which are essential for solving the linear system (6). The solution can be found by conventional iterative methods, where tensor algebra operations are performed on TT-formatted objects instead of full-size ones. In this paper, the AMEn algorithm was used, which is specifically optimised for the TT format [7].

Another important fact about matrix multiplication in TT format is that it results in a TT matrix with ranks equal to the sum of the ranks of the arguments. To prevent rank growth, TT rounding is used after each multiplication [15], which is an algorithm for finding the lowest rank approximation with a fixed accuracy.

The most common way of compressing arbitrary vectors is so called QTT (quantized tensor train) format, where all $n_k = 2$. In this work, QTT is used where possible.

3.3 Notation summary

In this article the following notation is used:

Object	Notation
Vector	\mathbf{x}
Matrix	\mathbf{A}
Vector element	x_i
Matrix element	A_{ij}
TT vector	X
TT matrix	A
TT core	\mathcal{X}_k
TT core «slice»	$\mathcal{X}_k(i_k)$

Each object, its TT representation and cores are denoted by the same letter in different fonts. Matrix elements may also be identified by lower case letters if the meaning is obvious from the context.

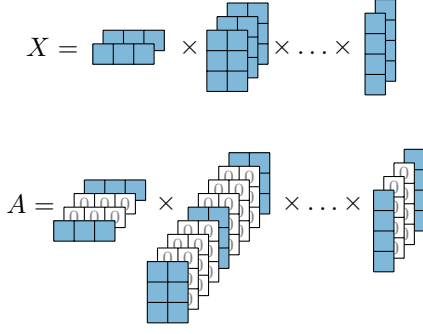


Figure 4: TT representation X of a vector \mathbf{x} with cores \mathcal{X}_i turned into TT matrix A representing a diagonal matrix $A_{ij} = \delta_{ij} \mathbf{x}_i$ by adding zero-layers into cores where $i_k \neq j_k$.

A is the matrix with $M = m_1 \times \dots \times m_{d_1}$ blocks of size $N = n_1 \times \dots \times n_d$. If one of the first d_1 pairs of indices i_k, j_k are not equal, this means that the element is outside one of the blocks, so it is equal to zero. If an element is inside a block, i.e. $i_k = j_k$ for $k = 1, \dots, d_1$, then this element is the same as in X .

Toeplitz matrix A of size N can be defined by a vector \mathbf{a} of size $2N - 1$: $A_{ij} = a_{i-j}$. If TT format of \mathbf{a} is known, TT cores of A can be found as shown in [12].

3.7 Elementary functions in TT format

A vector of samples of any smooth continuous function $f(x)$ can be constructed in the TT format using TT Cross algorithm. However, the cores obtained this way may not be optimal, since TT Cross is an iterative algorithm with random initial guess. Equidistant samples of some elementary functions can be found analytically in TT format with very small TT ranks. In this article $\sin(x)$, $\cos(x)$ and $\exp(ix)$ are used. These functions are implemented in the `ttpy` library, although their published description could not be found.

Consider the vector $\mathbf{x}_n = \sin(\alpha n + \varphi)$ where $n = 0, 1, \dots, N$. If $N = n_1 \dots n_d$, such vector can be found if the form of d -dimensional TT vector. To do this, we will consider the following matrix identities:

$$\begin{aligned} \begin{bmatrix} \cos(nx) & \sin(nx) \end{bmatrix} \cdot \begin{bmatrix} \cos(mx) & \sin(mx) \\ -\sin(mx) & \cos(mx) \end{bmatrix} &= \\ = \begin{bmatrix} \cos((n+m)x) & \sin((n+m)x) \end{bmatrix} & \end{aligned} \quad (16)$$

$$\begin{aligned} \begin{bmatrix} \cos(nx) & \sin(nx) \end{bmatrix} \cdot \begin{bmatrix} \sin(mx + \varphi) \\ \cos(mx + \varphi) \end{bmatrix} &= \\ = \sin((n+m)x + \varphi) & \end{aligned} \quad (17)$$

This allows constructing cores \mathcal{X}_k of vector \mathbf{x} as:

$$\begin{aligned} \mathcal{X}_1(i_1) &= \begin{bmatrix} \cos(i_1 \alpha N_{d-1}) & \sin(i_1 \alpha N_{d-1}) \end{bmatrix} \\ \mathcal{X}_k(i_k) &= \begin{bmatrix} \cos(i_k \alpha N_{d-k}) & \sin(i_k \alpha N_{d-k}) \\ -\sin(i_k \alpha N_{d-k}) & \cos(i_k \alpha N_{d-k}) \end{bmatrix}, \\ k &= 2, \dots, d-1 \end{aligned} \quad (18)$$

$$\mathcal{X}_d(i_d) = \begin{bmatrix} \sin(i_d \alpha + \varphi) \\ \cos(i_d \alpha + \varphi) \end{bmatrix}$$

where $N_k = n_1 \cdot n_2 \cdot \dots \cdot n_k$. TT ranks of this vector are $r_k = 2$. Replacing (18) with (16) and (17) gives:

$$\mathbf{x}_n = \sin((i_1 N_{d-1} + \dots + i_d) \alpha + \varphi) \quad (19)$$

which is the desired $\sin(\alpha n + \varphi)$ according to (8).

Cosine can easily be constructed as $\cos(\alpha n + \varphi) = \sin(\alpha n + \varphi + \pi/2)$ and the exponent $\exp(\alpha n + \varphi)$ can be constructed by the Euler's formula.

4 Diffraction matrix in TT form

To solve the linear system (6) using the AMEn algorithm, we need to find a TT representation of both the matrix $A = I - P_b Y D X$ and the vector \mathbf{a}^{inc} . Once the linear system is solved, to find a diffracted field we need to find the matrix $B = T Y D X$ (see 4). This can be done by the TT cross, but directly evaluating A_{ij} or B_{ij} elements requires a number of operations proportional to their full size N . To preserve the logarithmic complexity, all matrices P_b, Y, D, X and T must be decomposed separately and then multiplied in TT format. TT rounding must be performed after each multiplication to prevent rank growth.

As mentioned above, the TT Cross only works well with smooth tensors. Although the tensors listed above are regularly structured, they are defined by discontinuous functions. For example, a direct application of the TT Cross to the diagonal matrix Y would most likely result in a zero matrix decomposition, since most of its elements are zeros. To find compact TT representations, individual structural features of vectors and matrices have been exploited.

QTT format was used, so all the vector cores have two layers and matrix cores have four layers. All the matrices except T are square with size of $2 \cdot N_F \cdot N_S = 2^{d_F + d_S + 1}$, where $N_F = 2^{d_F}$ is the number of Fourier harmonics considered, and $N_S = 2^{d_S}$ is the number of grating layer slices. The vectors of the diffraction order amplitudes $\mathbf{a}_n^\pm(z_p)$ are arranged in the following way: n is the inner fastest changing index, p is the middle index, \pm is the outer slowest changing index.

Let us denote multiindices:

$$\mathbf{a}_n^\pm(z_p) = A_{\pm p_1 \dots p_{d_S} n_1 \dots n_{d_F}} \quad (20)$$

where A is the TT representation of \mathbf{a} , $\overline{n_1 \dots n_{d_F}}$ and $\overline{p_1 \dots p_{d_S}}$ are n and p in binary respectively. With this indexing, the first core of all amplitude vectors in the TT format will be called *direction core* with the first layer being selected for \mathbf{a}^+ and the second layer for \mathbf{a}^- . The next d_S cores are called *layer cores*, and the last d_F are called *order cores*:

$$\begin{aligned} \mathbf{a}_n^\pm(z_p) &= \underbrace{\mathcal{A}_1(\pm)}_{\text{direction core}} \underbrace{\mathcal{A}_2(p_1) \dots \mathcal{A}_{d_S+1}(p_{d_S})}_{\text{layer cores}} \cdot \\ &\quad \cdot \underbrace{\mathcal{A}_{d_S+2}(n_1) \dots \mathcal{A}_{d_S+d_F+1}(n_{d_F})}_{\text{order cores}} \end{aligned} \quad (21)$$

4.1 Vector \mathbf{a}^{inc}

Incidence is a plane wave with wave vector \mathbf{k}_0 propagating only in negative direction, thus $\mathbf{a}_n^{\text{inc},+}(z_p) = 0$ and $\mathbf{a}_{n \neq 0}^{\text{inc},-}(z_p) = 0$. All non-zero elements:

$$\mathbf{a}_0^{\text{inc},-}(z_p) = \exp(ik_{z0}\Delta z_p) \quad (22)$$

where $\Delta z_p = (N_S - p - 1/2) dh$.

This vector can be constructed in three steps. First, we may find a TT representation of all non-zero elements, that are equidistant exponent samples $\exp(\alpha n + \varphi)$, as shown above with $\alpha = -ik_{z0} dh$ and $\varphi = ik_{z0} dh (N_S - 1/2)$. The cores obtained are the layer cores.

Secondly, the order cores should be added:

$$\mathcal{A}_{k+d_S+1}(n_k) = \begin{cases} 1, & n_k \text{ fits } n = 0 \\ 0, & \text{otherwise} \end{cases} \quad (23)$$

so that $\mathbf{a}_{n \neq 0} = 0$, and $\mathbf{a}_{n=0}$ is defined by the layer cores.

Finally, the direction core $\mathcal{A}_1(+)=0$, $\mathcal{A}_1(-)=1$ should be added so that all positively propagating waves have zero amplitude.

4.2 Identity matrix and \mathbf{X}

Identity matrix \mathbf{I} in QTT format looks very simple. All the ranks $r_k = 1$, and cores have four elements: $\mathcal{I}_k(0,0) = \mathcal{I}_k(1,1) = 1$ and $\mathcal{I}_k(0,1) = \mathcal{I}_k(1,0) = 0$.

Matrix \mathbf{X} can be constructed from the identity matrix using the Kronecker product:

$$\mathbf{X} = \begin{bmatrix} 1 & 1 \\ 1 & 1 \end{bmatrix} \otimes \mathbf{I} \quad (24)$$

4.3 Matrix \mathbf{Y}

\mathbf{Y} is a diagonal matrix with non-zero elements:

$$\mathbf{Y}_{pn,pn} = \frac{1}{k_{zn}} \quad (25)$$

To construct the TT representation of \mathbf{Y} we used the TT Cross to evaluate vector $\mathbf{x}_n = 1/k_{zn}$ of size N_F , then tiled it $2N_S$ times, and finally transformed it into a diagonal matrix.

4.4 Matrix \mathbf{D}

Matrix \mathbf{D} is a block-diagonal matrix with $2N_S$ equal Toeplitz blocks:

$$\mathbf{D}_{nm}^{\text{block}} = \llbracket \varepsilon(x) \rrbracket_{n-m} \quad (26)$$

As mentioned above, Toeplitz matrices in the TT format can be constructed from TT vector containing its anti-diagonal elements. If a Fourier transform of the grating permittivity spatial distribution is known, a TT representation of the vector $\llbracket \varepsilon \rrbracket$ can be found using the TT Cross algorithm.

If the TT matrix $\mathbf{D}^{\text{block}}$ is known, it can be tiled $2N_S$ times and transformed into the block-diagonal matrix \mathbf{D} as shown in (15).

A simple lamellar grating is defined as:

$$\varepsilon(x) = \begin{cases} \varepsilon_{\text{max}}, & -\frac{\gamma\Lambda}{2} < x < \frac{\gamma\Lambda}{2} \\ \varepsilon_{\text{min}}, & \text{otherwise,} \end{cases} \quad (27)$$

where Λ is the grating period, and γ is the *filling factor*. The Fourier amplitudes analytically write

$$\llbracket \varepsilon \rrbracket_n = \begin{cases} (\varepsilon_{\text{max}} - \varepsilon_{\text{min}}) \cdot \frac{\sin(\frac{\pi n \gamma}{\Lambda})}{\pi n}, & n \neq 0 \\ (\varepsilon_{\text{max}} - \varepsilon_{\text{min}}) \cdot \gamma + \varepsilon_{\text{min}}, & n = 0 \end{cases} \quad (28)$$

In order to use the TT Cross, diagonal elements were evaluated separately, turned into a diagonal TT matrix and added to the obtained Toeplitz matrix.

4.5 Matrix \mathbf{P}_b

The matrix \mathbf{P}_b represents propagation of the waves emitted by the generalized currents in each slice between different slices. It consists of two blocks:

$$\mathbf{P}_b = \begin{bmatrix} \mathbf{P}_b^+ & \mathbf{0} \\ \mathbf{0} & \mathbf{P}_b^- \end{bmatrix} \quad (29)$$

where:

$$\left(\mathbf{P}_b^+ \right)_{nm}(p,q) = \begin{cases} \delta_{nm} e^{ik_{zn} \cdot dh(p-q)}, & p > q \\ \frac{1}{2} \delta_{nm}, & p = q \\ 0, & p < q \end{cases} \quad (30)$$

$$\mathbf{P}_b^- = \left(\mathbf{P}_b^+ \right)^T \quad (31)$$

If \mathbf{P}_b^+ is known, then:

$$\mathbf{P}_b = \begin{bmatrix} 1 & 0 \\ 0 & 0 \end{bmatrix} \otimes \mathbf{P}_b^+ + \begin{bmatrix} 0 & 0 \\ 0 & 1 \end{bmatrix} \otimes \left(\mathbf{P}_b^+ \right)^T \quad (32)$$

To simplify the computation of \mathbf{P}_b^+ the indices n and p can be permuted, i.e. the order indices n_k will change slower than p_k . This permutation turns \mathbf{P}_b^+ into a block-diagonal matrix with Toeplitz blocks $\left(\mathbf{P}_b^+ \right)_n$ being:

$$\left[\begin{array}{cccccc} \frac{1}{2} & 0 & \dots & \dots & 0 & \\ e^{ik_{zn}dh} & \ddots & \ddots & & \vdots & \\ e^{2ik_{zn}dh} & \ddots & \ddots & \ddots & \vdots & \\ \vdots & \ddots & \ddots & \ddots & 0 & \\ e^{(N_S-1)ik_{zn}dh} & \dots & e^{2ik_{zn}dh} & e^{ik_{zn}dh} & \frac{1}{2} & \end{array} \right] \quad (33)$$

The \mathbf{P}_b^+ in this form can be constructed in four steps. First, we compute the tensor of exponent matrix blocks as a Kronecker product:

$$i dh \cdot \begin{bmatrix} 0 & 0 & \dots & \dots & 0 \\ 1 & \ddots & \ddots & & \vdots \\ 2 & \ddots & \ddots & \ddots & \vdots \\ \vdots & \ddots & \ddots & \ddots & 0 \\ N_S - 1 & \dots & 2 & 1 & 0 \end{bmatrix} \otimes \begin{bmatrix} k_{z, \frac{-N_F}{2}} \\ \vdots \\ k_{z, \frac{N_F}{2} - 1} \end{bmatrix} \quad (34)$$

where both the matrix and the vector are in TT format. The matrix can be analytically decomposed into TT format as a lower triangular Toeplitz matrix, and the vector \mathbf{k}_z can be defined using the TT Cross as previously.

Second, the exponentiation function should be applied element-wise by TT Cross. The resulting tensor of matrix blocks is the same as (33) in the lower part. But on the main diagonal and higher there are ones instead of 1/2 and zeros respectively. So, thirdly, we have to subtract Toeplitz matrix defined by anti-diagonal vector $[0, \dots, 0, \frac{1}{2}, 1, \dots, 1]$ from each block.

Then, the computed tensor of diagonal blocks of \mathbf{P}_b^+ have to be turned into block-diagonal matrix as shown in (15).

Since \mathbf{P}_b^+ is constructed with permuted p_k and n_k indices, we need to swap them back. The TT framework provides an index permutation algorithm, but it is relatively slow. The fastest way to do the permutation is to swap order and layer cores in the first step, and then perform all operations with permuted indices. For example, the block diagonal matrix construction algorithm should be modified so that zero layers are added to the last cores instead of the first.

4.6 Matrix \mathbf{T}

The matrix \mathbf{T} is a non-square matrix of size $2N_F \times 2N_F N_S$. When multiplied by the amplitude vector of the self-consistent field calculated in each slice, it gives a vector of the resulting outgoing field amplitudes at the grating layer boundaries.

$$\mathbf{T} = \begin{bmatrix} \mathbb{0} & \mathbf{T}^+ \\ \mathbf{T}^- & \mathbb{0} \end{bmatrix} \quad (35)$$

Blocks \mathbf{T}^\pm are in anti-diagonal positions.

$$\mathbf{T}_{nm}^\pm(p) = \delta_{nm} \exp(ik_{zn} \Delta_p^\pm) \quad (36)$$

where $\Delta_p^+ = dh(N_S - p + 1/2)$, $\Delta_p^- = dh(p - 1/2)$. The construction of this matrix in the TT format is almost identical to R with the exception that \mathbf{T} is non-square, to the tensor mode sizes corresponding to the layer indices are set to one.

5 Numerical examples

To check that the accelerated method worked correctly, it was compared with conventional FMM and unmodified GSM. The results agreed within a given accuracy. Figure 5 shows how the new method converges to a given accuracy. For further experiments, the tolerance in terms of $\|\mathbf{a}\|$ was set to 10^{-6} .

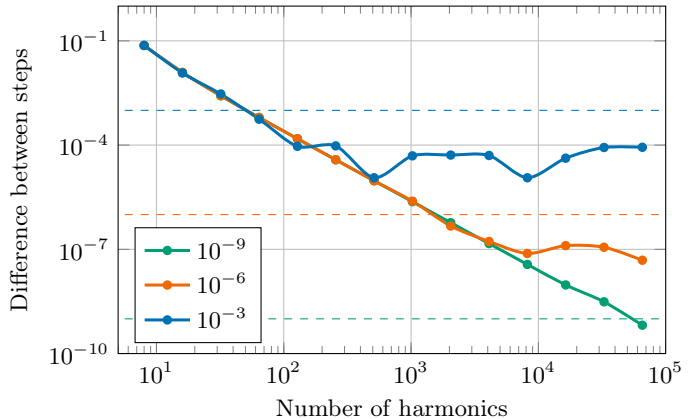


Figure 5: Convergence of the new algorithm (GSM TT) with respect to the number of considered Fourier harmonics N_F for varying preset accuracy (indicated by dashed lines).

To evaluate the computational complexity of the new method, it was tested on a single scale lamellar diffraction grating. Figure 6 compares the algorithm runtime and memory usage with unmodified GSM. N_L has been set equal to N_F to maintain accuracy.

The results shown should only be considered from an asymptotic point of view, as all methods are implemented differently. However, it is clear that the GSM TT requires exponentially less time and memory than conventional methods. This allows a much larger number of spatial field harmonics to be considered, and thus diffraction by more complex structures to be simulated.

To test whether the method can simulate diffraction on multi-scale structures of different thicknesses, we considered binary gratings consisting of multiple pixels with different random widths (as shown in Fig. 1). The distance between the centres of all pixels is fixed and equal to the incident wavelength λ . Figure 7 shows the convergence of the new method when considering gratings with increasing period. Figure 8 shows the convergence when considering gratings with a fixed period of 10λ and varying grating thickness.

When enough harmonics are considered, all simulations converge to an accuracy not exceeding the TT format default of 10^{-6} . The rate of convergence resembles the slope $O(x^{-2})$. It is worth noting that in most simulations the difference between the steps first increases and then decreases. This is due to the exponentially increasing step size along the horizontal axis.

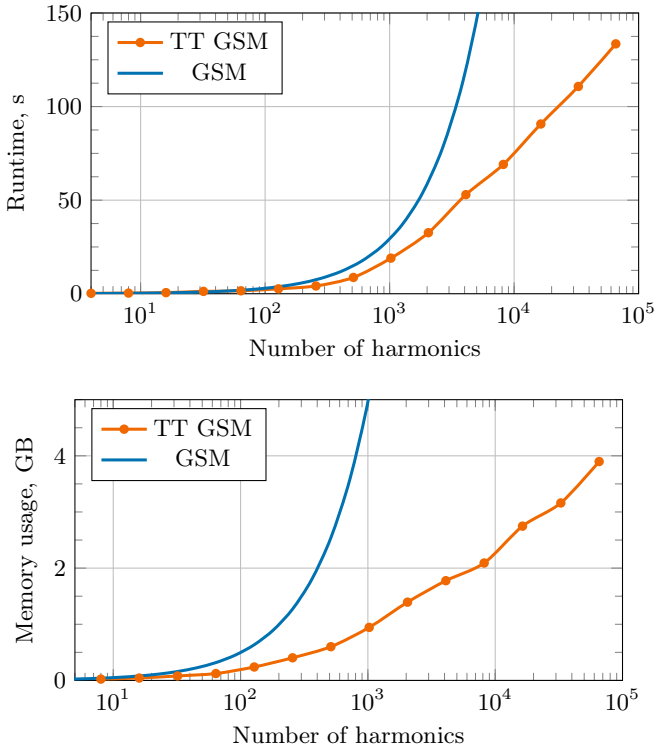


Figure 6: New algorithm (GSM TT) running time and memory usage compared to the unmodified GSM.

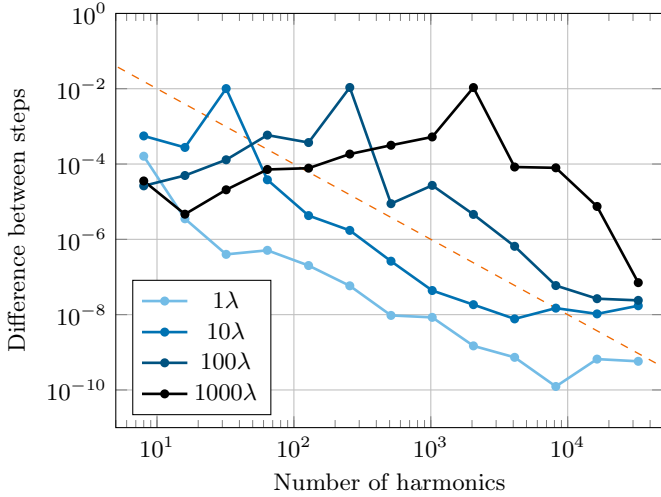


Figure 7: Convergence of the new method for two-scale gratings. The smaller scale equals to the wavelength λ , the larger scale varies from 1λ to 1000λ . Grating thickness is set to 0.5λ . The value on vertical axis is the difference between zero harmonic amplitudes calculated with adjacent d_F . Dashed line indicates the functional dependence $O(x^{-2})$.

6 Discussion and conclusion

Although the Generalized Sourced Method is well conditioned, the use of the Tensor Train may lead to numerical

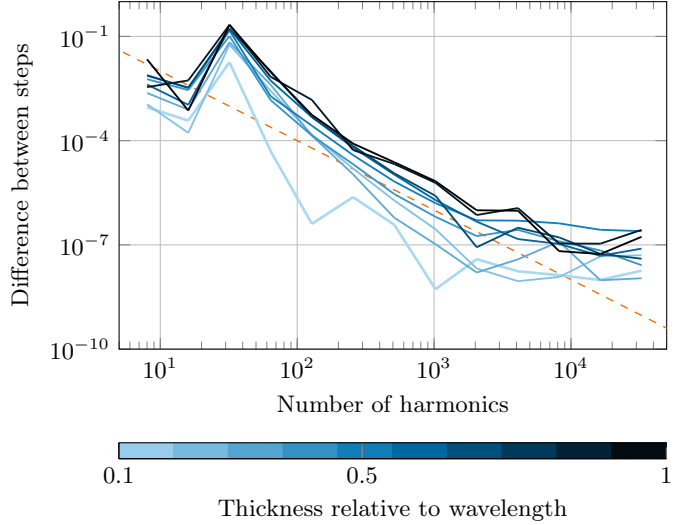


Figure 8: Convergence of the new method for two-scale gratings with period 10λ . Grating thickness varies in range from 0.1λ to λ . The value on vertical axis is the difference between zero harmonic amplitudes calculated with adjacent d_F . Dashed line indicates the functional dependence $O(x^{-2})$.

instability in the case of extremely large N_F . For the most part, TT algorithms are stably formulated with analytically defined error bounds. The only potentially problematic method is the TT Cross, as it requires the tensors considered to be «sufficiently smooth», a term that isn't properly defined.

Instability can be caused by two main factors. The first cause of the inaccuracy of the TT approximation of k_{zn} . This vector contains both real and complex values representing propagating and evanescent waves respectively. As N_F increases, an increasing number of evanescent waves with higher $\text{Im}(k_{zn})$ are considered. The accuracy of the TT Cross approximation is defined in terms of the vector norm. Consequently, when $|k_{z,0}| \ll |k_{z,N_F}|$, the most significant zero-mode is approximated with a large error.

This problem can be solved with a relatively simple workaround. Unlike most tensors used in TT GSM, k_{zn} is small enough to fit within the memory constraints of a typical computer, even for very large values of N_F . This allows its TT representation to be found directly from its full form using the TT SVD [15].

Another potential cause of source is instability in defining of the \mathbf{P}_b matrix. As N_F increases, most of its elements become close to zero, and evanescent waves with large $\text{Im}(k_{zn})$ decay to machine zero within a single grating slice. In such scenarios, \mathbf{P}_b becomes close to being diagonal, so the TT-Cross may struggle to provide an accurate approximation.

A partial solution to this issue can be achieved by considering smoother symmetric blocks, $\mathbf{P}_b^+ + (\mathbf{P}_b^+)^T + \mathbf{I}$, instead of the lower triangular ones. While this workaround improves the stability of some examples, this approach

may not be reliable in general.

Note that these two issues only arise when the number of evanescent waves considered is several orders of magnitude greater than the number of propagating waves. This does not typically occur in practical calculations.

In conclusion, in this work we have accelerated the GSM with adapted TT decomposition algorithms and demonstrated the ability of the resulting method to yield solutions to large-period multiscale grating diffraction problems with $O(\log N)$ asymptotic numerical complexity and memory.

Acknowledgements

The work was supported by the Russian Science Foundation, grant No.22-11-00153. The authors are grateful to the Professor Ivan Oseledets for advice on the use of his codes.

References

- [1] Sensong An, Bowen Zheng, Mikhail Y. Shalaginov, Hong Tang, Hang Li, Li Zhou, Jun Ding, Anuradha Murthy Agarwal, Clara Rivero-Baleine, Myungkoo Kang, Kathleen A. Richardson, Tian Gu, Juejun Hu, Clayton Fowler, and Hualiang Zhang. Deep learning modeling approach for metasurfaces with high degrees of freedom. *Optics Express*, 28(21):31932, October 2020.
- [2] N. Anselmi, G. Oliveri, L. Poli, A. Polo, P. Rocca, M. Salucci, and A. Massa. *Breaking the Curse of Dimensionality in Electromagnetics Design Through Optimization Empowered by Machine Learning*, pages 81–104. 2023.
- [3] Tryfon Antonakakis, Fadi Issam Baida, Abderrahmane Belkhir, Kirill Cherednichenko, Shane Cooper, Richard Craster, Guillaume Demésy, John Desanto, Gérard Granet, Boris Gralak, Sébastien Guenneau, Daniel Maystre, André Nicolet, Brian Stout, Frédéric Zolla, Benjamin Vial, and Evgeni Popov. *Gratings: Theory and Numeric Applications*. AMU (PUP), December 2012.
- [4] M Bonnet, F Collino, E Demaldent, A Imperiale, and L Pesudo. A hybrid method combining the surface integral equation method and ray tracing for the numerical simulation of high frequency diffraction involved in ultrasonic ntd. *Journal of Physics: Conference Series*, 1017:012007, May 2018.
- [5] Jean Chandezon and Gérard Granet. Diffraction by gratings: from the c-method to the stochastic c-method. *Journal of the Optical Society of America A*, 41(9):1675, August 2024.
- [6] W.C. Chew. *Waves and Fields in Inhomogeneous Media*. Electromagnetic Waves Series. IEEE Press, 1995.
- [7] Sergey V. Dolgov and Dmitry V. Savostyanov. Alternating minimal energy methods for linear systems in higher dimensions. *SIAM Journal on Scientific Computing*, 36(5):A2248–A2271, jan 2014.
- [8] Hong-Wei Gao, Xi-Min Xin, Qi Jian Lim, Shu Wang, and Zhen Peng. Efficient full-wave simulation of large-scale metasurfaces and metamaterials. *IEEE Transactions on Antennas and Propagation*, 72(1):800–811, January 2024.
- [9] Sergei A. Goreinov, Eugene E. Tyrtysnikov, and Nikolai Zamarashkin. A theory of pseudoskeleton approximations. *Linear Algebra and its Applications*, 261:1–21, 1997.
- [10] Florian Hudelist, Andrew J. Waddie, and Mohammad R. Taghizadeh. Analysis of crossed gratings with large periods and small feature sizes by stitching of the electromagnetic field. *Journal of the Optical Society of America A*, 26(12):2648, November 2009.
- [11] Tyler W. Hughes, Momchil Minkov, Victor Liu, Zongfu Yu, and Shanhui Fan. A perspective on the pathway toward full wave simulation of large area metalenses. *Applied Physics Letters*, 119(15), October 2021.
- [12] Vladimir A. Kazeev, Boris N. Khoromskij, and Eugene E. Tyrtysnikov. Multilevel toeplitz matrices generated by tensor-structured vectors and convolution with logarithmic complexity. *SIAM Journal on Scientific Computing*, 35(3):A1511–A1536, 2013.
- [13] Clément Majorel, Christian Girard, Arnaud Arbouet, Otto L. Muskens, and Peter R. Wiecha. Deep learning enabled strategies for modeling of complex aperiodic plasmonic metasurfaces of arbitrary size. *ACS Photonics*, 9(2):575–585, January 2022.
- [14] V. Medvedev, A. Erdmann, and A. Roskopf. Modeling of near-and far-field diffraction from euv absorbers using physics-informed neural networks. In *2023 Photonics & Electromagnetics Research Symposium (PIERS)*, pages 297–305, 2023.
- [15] I. V. Oseledets. Tensor-train decomposition. *SIAM Journal on Scientific Computing*, 33(5):2295–2317, 2011.
- [16] Ivan Oseledets and Eugene Tyrtysnikov. Tt-cross approximation for multidimensional arrays. *Linear Algebra and its Applications*, 432(1):70–88, 2010.
- [17] R. Petit, editor. *Electromagnetic Theory of Gratings*. Springer Berlin Heidelberg, 1980.
- [18] Mohammad Mahdi Salary, Ali Forouzmand, and Hossein Mosallaei. Model order reduction of large-scale metasurfaces using a hierarchical dipole approximation. *ACS Photonics*, 4(1):63–75, December 2016.

- [19] Sulagna Sarkar, Anqi Ji, Zachary Jermain, Robert Lipton, Mark Brongersma, Kaushik Dayal, and Hae Young Noh. Physics-informed machine learning for inverse design of optical metamaterials. *Advanced Photonics Research*, 4(12), October 2023.
- [20] Sebastian A. Schulz, Rupert F. Oulton, Mitchell Kenney, Andrea Alù, Isabelle Staude, Ayesheh Bashiri, Zlata Fedorova, Radoslaw Kolkowski, A. Femius Koenderink, Xiaofei Xiao, John Yang, William J. Peveler, Alasdair W. Clark, George Perakis, Anna C. Tasolamprou, Maria Kafesaki, Anastasiia Zaleska, Wayne Dickson, David Richards, Anatoly Zayats, Haoran Ren, Yuri Kivshar, Stefan Maier, Xianzhong Chen, Muhammad Afnan Ansari, Yuhui Gan, Arseny Alexeev, Thomas F. Krauss, Andrea Di Falco, Sylvain D. Gennaro, Tomás Santiago-Cruz, Igal Brener, Maria V. Chekhova, Ren-Min Ma, Viola V. Vogler-Neuling, Helena C. Weigand, Ülle-Linda Talts, Irene Occhiodori, Rachel Grange, Mohsen Rahmani, Lei Xu, S. M. Kamali, E. Arababi, Andrei Faraon, Anthony C. Harwood, Stefano Vezzoli, Riccardo Sapienza, Philippe Lalanne, Alexandre Dmitriev, Carsten Rockstuhl, Alexander Sprafke, Kevin Vynck, Jeremy Upham, M. Zahirul Alam, Israel De Leon, Robert W. Boyd, Willie J. Padilla, Jordan M. Malof, Alope Jana, Zijin Yang, Rémi Colom, Qinghua Song, Patrice Genevet, Karim Achouri, Andrey B. Evlyukhin, Ulrich Lemmer, and Ivan Fernandez-Corbaton. Roadmap on photonic metasurfaces. *Applied Physics Letters*, 124(26), June 2024.
- [21] H. Schwerdtfeger. The theory of matrices, by f. r. gantmacher. chelsea, new york, 1959. vol. i. x 374 pages; vol. ii. ix 276 pages. \$6.00 per volume. *Canadian Mathematical Bulletin*, 4(1):82–85, 1961.
- [22] A.A. Shcherbakov, O. Shavdina, A.V. Tishchenko, C. Veillas, I. Verrier, O. Dellea, and Y. Jourlin. Optical diffraction by ordered 2d arrays of silica microspheres. *Journal of Quantitative Spectroscopy and Radiative Transfer*, 189:37–42, March 2017.
- [23] Alexey Shcherbakov and Alexandre Tishchenko. Fast numerical method for modelling one-dimensional diffraction gratings. *Quantum Electronics*, 40:538, 08 2010.
- [24] Alexey A. Shcherbakov and Alexandre V. Tishchenko. New fast and memory-sparing method for rigorous electromagnetic analysis of 2d periodic dielectric structures. *Journal of Quantitative Spectroscopy and Radiative Transfer*, 113(2):158–171, 2012.
- [25] Jinhie Skarda, Rahul Trivedi, Logan Su, Diego Ahmad-Stein, Hyoungghan Kwon, Seunghoon Han, Shanhui Fan, and Jelena Vučković. Low-overhead distribution strategy for simulation and optimization of large-area metasurfaces. *npj Computational Materials*, 8(1), April 2022.
- [26] A. V. Tishchenko. Generalized source method: New possibilities for waveguide and grating problems. *Optical and Quantum Electronics*, 32(6):971–980, Aug 2000.